Journal of Magnetic Resonance 331 (2021) 107049

Contents lists available at ScienceDirect

Journal of Magnetic Resonance

journal homepage: www.elsevier.com/locate/jmr

Accelerating ^{15}N and ^{13}C R_1 and $R_{1\rho}$ relaxation measurements by multiple pathway solid-state NMR experiments

Jacqueline Tognetti [a,b], W. Trent Franks [a,b], Angelo Gallo [b], Józef R. Lewandowski [b,*]

[a] Department of Physics, University of Warwick, Coventry CV4 7AL, United Kingdom
[b] Department of Chemistry, University of Warwick, Coventry CV4 7AL, United Kingdom

ARTICLE INFO

Article history:
Received 8 July 2021
Revised 9 August 2021
Accepted 11 August 2021
Available online 21 August 2021

Keywords:
Solid-state NMR
Magic angle spinning
NMR relaxation
Staggered acquisition

ABSTRACT

Magic angle spinning (MAS) Solid-state NMR is a powerful technique to probe dynamics of biological systems at atomic resolution. R_1 and $R_{1\rho}$ relaxation measurements can provide detailed insight on amplitudes and time scales of motions, especially when information from several different site-specific types of probes is combined. However, such experiments are time-consuming to perform. Shortening the time necessary to record relaxation data for different nuclei will greatly enhance practicality of such approaches. Here, we present staggered acquisition experiments to acquire multiple relaxation experiments from a single excitation to reduce the overall experimental time. Our strategy enables one to collect ^{15}N and ^{13}C relaxation data in a single experiment in a fraction of the time necessary for two separate experiments, with the same signal to noise ratio.

1. Introduction

Quantifying biomolecular motions plays a fundamental role towards the understanding of biophysical processes as modulated by protein dynamics. In solid-state NMR the range of time scales that can be detected by relaxation experiments is not limited by overall tumbling as in solution-state NMR. Molecular processes that are characteristic of protein functions like enzymatic catalysis, protein folding, and ligand binding are on the order of μs-ms which is the same as the timescale amenable for study by solid state NMR using relaxation techniques. NMR relaxation [1–4] experiments, however, are time-consuming considering the very long delays necessary to adequately sample relaxation times and the large number of scans often required to achieve appropriate signal to noise ratios for challenging systems [5–7]. In particular, ^{15}N R_1 can be < 0.02 s^{-1} requiring relaxation delays up to ~ 50 s (on top of the recycling delay). In addition, the description of protein motions spanning a wide range of time scales, often requires access to multiple independent probes in order to obtain a detailed view of dynamics, *e.g.* joint use of ^{15}N and $^{13}C'$ relaxation leads to an improved view of backbone dynamics [2]. Finally, some experiments require multiple measurements on the same probes under different conditions, *e.g.* relaxation dispersion where $R_{1\rho}$ is measured as a function of the applied field strength of the spin-locking pulses [6,8] or variable temperature measurements [9,10]. Overall, this means that quantification of protein dynamics may involve recording many time-consuming experiments, which limits the wide adoption of this powerful methodology. In order to make such studies more widespread, it will be thus useful to develop approaches which reduce the overall experimental time required.

Paramagnetic doping is a widely applicable approach to reduce the recycling times in solid-state NMR experiments [11–14]. However, the addition of paramagnetic dopants will also change the measured ^{15}N and ^{13}C relaxation rates [6], with the contribution related to the distance of the monitored site to the paramagnetic centre often dominating the contributions from the local dynamics [15]. Similarly to paramagnetic doping, for a number of reasons, selective excitation methods popular in solution NMR [16,17] are not yet appropriate for accelerating quantitative relaxation measurements in solids.

Solid-state NMR experiments could be devised to use the available initial polarization more efficiently than standard approaches, *e.g.* time-shared experiments and sequential acquisition experiments that exploit orphaned polarization. Time-shared experiments [18,19] pass the signal through multiple polarization pathways and collect all experiments at once. In the Dual Acquisition Magic Angle Spinning (DUMAS) [20] acquisition scheme, the acquisition of the nitrogen and carbon-based experiments are separated in time (with polarization from one source being stored) to eliminate signal overlap from the separate experiments. This

* Corresponding author.
E-mail address: J.R.Lewandowski@warwick.ac.uk (J.R. Lewandowski).

https://doi.org/10.1016/j.jmr.2021.107049
1090-7807/

multiple acquisition scheme has been also used for ^{1}H detection [21], for detection of orphaned polarization [22], for use with multiple receivers [21], and for mixed dimensionality multi-receiver experiments [23]. Sequential acquisition results in a small time-penalty for the second acquisition but the time loss is usually very short compared to the recovery time.

In this study, we present experiments to measure ^{15}N/^{13}C $R_{1\rho}$ [1,2,8,24,25] and R_1 [26,27], with staggered acquisition ^{1}H-detected experiments. We demonstrate that relaxation measurements on a model protein obtained with staggered and standard acquisition are the same within the experimental error. We quantify sensitivity of the multiple acquisition experiments and the overall experimental time gains with respect to the standard experiments.

2. Experimental

Uniformly [^{1}H,^{13}C,^{15}N] labelled GB1 was prepared as described previously [28] and doped with 4,4-dimethyl-4-silapentane-1-sulfonic acid (DSS) as an internal standard. ~ 0.5 mg of hydrated microcrystalline protein was centrifuged into a 0.7 mm solid-state NMR rotor using a device developed in-house [29].

All experiments were performed on a Bruker Avance III spectrometer, using a Bruker HCND Probe operating in triple resonance at 700.13 ^{1}H Larmor frequency and sample spinning rate of 100 kHz +/- 3 Hz. The experiments were carried out at a nominal temperature of 281.2 K (based on external calibration, calculated by the difference between the water and sodium 3-(trimethylsilyl)propane-1-sulfonate (DSS) peaks) using a gas flow of 400 L/h [30,31]. The nutation frequencies for the 90° pulses were calibrated so that ^{1}H is at 2 μs (ν_1 = 125 kHz); ^{13}C, 2.5 μs (ν_1 = 100 kHz); and ^{15}N, 4.15 μs (ν_1 = 60.24 kHz). The ^{15}N carrier radiofrequency (RF) was centred at 120 ppm, while the ^{13}C was placed at 55 ppm and 175 ppm, for $^{13}C^{\alpha}$ and ^{13}C' respectively. The carbon frequency was moved by changing the carrier frequency in the Bruker pulse code using pre-determined constants. The ^{1}H carrier was placed near the water frequency (~4.7 ppm) for the standard ^{15}N $R_{1\rho}$ relaxation experiment. Each ^{1}H free induction decay was acquired for 30 ms with a spectral width of 35 ppm with 16 coadded transients. Both the ^{15}N and ^{13}C' dimensions for the $R_{1\rho}$ experiments were acquired with 82 rows with a dwell of 300 μs, with a spectral width of 47 ppm (^{15}N) and 19 ppm (^{13}C'), for a total of 12.6 ms in the indirect dimensions. In the hcαC'cαHα + hNH_N variant, both the ^{15}N and ^{13}C' dimensions were acquired with 72 rows with a dwell of 300 μs, maintaining the same spectral widths. The number of rows sampled in the indirect dimension of the two parts of the simultaneous experiment must be the same, but the spectral width is not restricted in this way. For the R_1 measurements ^{15}N and ^{13}C'dimensions were acquired with 64 rows with a dwell of 300 μs, with a spectral width of 47 ppm (^{15}N) and 19 ppm (^{13}C'), for a total of 9.6 ms in the indirect dimensions. The recovery delay was 2.5 s for all the $R_{1\rho}$ experiments and 1.5 s for the R_1 measurements. The States-TPPI method was employed for quadrature detection in the indirect dimensions [32]. Heteronuclear ^{1}H decoupling (~10 kHz WALTZ-64 [33]) was applied during t_1 evolution on ^{13}C, ^{15}N, and during the COSY-based transfers. Heteronuclear decoupling on the ^{13}C channel (~10 kHz WALTZ-64) was applied during both direct acquisitions, while ^{15}N heteronuclear decoupling (~10 kHz WALTZ-64) was only used for the HN acquisition. The MISSISSIPPI [34] solvent suppression scheme was applied with a spinlock field of ~ 50 kHz for four 20 ms intervals for the $R_{1\rho}$ and R_1 singleton experiments, and the R_1 staggered experiments. For the $R_{1\rho}$ staggered experiments the four MISSISSIPPI intervals were 20 ms for the first ^{13}C' pathway acquisition, and 7.5 ms for the subsequent ^{15}N pathway. All spinlock fields for the $R_{1\rho}$ experiments were calibrated to be ν_1 = 5 kHz by nutation; eleven points from 2 ms to 210 ms were collected. The spacing between points in the delay schedules for the R_1 measurements is based on the spacing of the Fibonacci sequence where appropriate beginning and ending times were chosen based on previous experience. The complete set of time-points used for both $R_{1\rho}$ and R_1 can be found in the supporting information.

Simultaneous cross-polarization (SIM-CP) [35] was used for the initial excitation of ^{13}C and ^{15}N, where the average ^{1}H field was ~ 130 kHz with a linear 15% ramp (85%-100%, from ~ 121.5 to 139.5 kHz) using a zero-quantum (ZQ) match condition transfer for both ^{13}C and ^{15}N, where both channels are irradiated at ~ 30 kHz, and the carrier is on resonance with the indicated resonance. The contact times for $^{13}C^{\alpha}$, ^{13}C' and ^{15}N were optimized on both the single and staggered pathway correlation experiments. The contact time was 2.1 ms for ^{1}H–^{13}C' CP and 150 μs for the ^{1}H–$^{13}C^{\alpha}$ CP. For the ^{1}H–^{15}N CP, the contact times were 2 ms and 1.7 ms for individual and staggered $R_{1\rho}$ measurements respectively. The ^{1}H pulse duration is set to the longest contact time of the two nuclei for SIM-CP. Polarization is always stored on the low-gamma nuclei after CP, no matter which CP time is longer, to provide the most flexibility in CP times. Our pulse sequence naming convention indicates all transfer steps in the sequence by nucleus name. An upper-case nucleus indicates that the chemical shift is evolved. A lower-case name indicates that polarization is transferred through, but there is no chemical shift evolution (this is sometimes designated with parentheses). A pulse sequence name with square braces where nucleus names are separated by commas indicates separate polarization pathways in the same experiment. In the text, we refer to these experiments with a "+" between the independent experiments.

Gaussian Q3 cascade pulses were calibrated for selective ^{13}C inversion where a 320 μs pulse gives a bandwidth of 10.5 kHz (~60 ppm) and 760 μs produces a bandwidth of 5.3 kHz (~30 ppm) for ^{13}C' and $^{13}C^{\alpha}$ respectively. For the selective $^{13}C^{\alpha}$–^{13}C' coherence transfer, the *J*-coupling delay (τ) was 3.5 ms in the $R_{1\rho}$ measurements and 3 ms in the R_1 measurements for the period were the $^{13}C^{\alpha}$ magnetization is transverse and 4.25 ms for the period where ^{13}C' is transverse. The pulse sequences, datasets, lists, compound pulse lists, and pulse shapes can be found online in the Mendeley Data: http://dx.https://doi.org/10.17632/x7kk4rkpj3.1.

All relaxation rates are reported at the 95% confidence level from 2000 steps of Monte Carlo error analysis [36].

3. Results and discussion

Quantification of protein dynamics based on relaxation rates relies on suppression of coherent effects that can obscure the information on the molecular motions encoded in the measured rates [4]. For example, in uniformly [^{1}H,^{13}C,^{15}N] labelled samples, spin diffusion [27,37,38] will lead to the averaging of the rates for nearby sites, compromising their site-specific nature. In addition, coherent effects can lead to additional decay of magnetisation compromising R_2 and $R_{1\rho}$ measurements [3,24]. However, the left-over anisotropic interactions, especially strong ^{1}H–^{1}H proton dipolar couplings, can be reduced by fast spinning and combined with deuteration and/or alternating labelling to effectively average out the interactions [27,38,39]. The exact conditions to attenuate the spin diffusion sufficiently so that it has a negligible effect on the site-specificity of the rates depends on the exact type of relaxation probes. For example, for ^{15}N nuclei spinning frequencies > 20 kHz are sufficient to obtain site-specific ^{15}N R_1 rates [38,40] and spinning rates > 60 kHz are sufficient to obtain site-specific ^{15}N $R_{1\rho}$ rates without the need for deuteration or any special labelling pat-

tern [24]. For ^{13}C' nuclei spinning frequencies > 60 kHz are adequate for recording site-specific $R_1/R_{1\rho}$ rates [2,27] but for the aliphatic carbons more demanding conditions need to be met: for ^{13}C$^{\alpha}$ either (1) a combination of alternate ^{13}C labelling, and extensive deuteration and 50–60 kHz spinning need to be employed for site specific R_1 measurements [39] or (2) a combination of alternate ^{13}C labelling and > 80 kHz spinning [29] or (3) > 100 kHz spinning for uniformly ^{13}C-labelled samples [29]. Alternate ^{13}C labelling is still required in fully protonated samples in order to collect site specific aliphatic ^{13}C $R_{1\rho}$ rates since many sidechain sites still show spin diffusion even at 100 kHz spinning in uniformly labelled samples [29].

Based on the above discussion recording ^{15}N and ^{13}C' R_1 and $R_{1\rho}$ relaxation rates in uniformly ^{15}N and ^{13}C labelled samples at 100 kHz spinning should result in measurements with negligible influence of coherent effects. In addition, under these conditions ^{1}H-detected spectroscopy in fully protonated samples is the most practical detection mode. Consequently, below we will explore a range of solutions for simultaneous measurements of ^{15}N and ^{13}C' relaxation rates using ^{1}H-detected experiments.

Constructing Multiple Acquisition Psuedo-3D experiments from 2D correlation experiments

To construct multiple pathway experiments, we will adapt 2D ^{1}H-detected correlation experiments into pseudo-3D experiments by adding relaxation periods at the appropriate places in the pulse sequence (Fig. 1**a,b and** Fig. 3**a,b**). For the ^{13}C' measurements, we found that a direct adaptation of the standard CP-based ^{1}H-detected ^{13}C–^{1}H correlation experiment was not sufficient. The final ^{13}C'–^{1}H transfer spreads the polarization to several nearby protons, causing reduction of the sensitivity and increasing the spectral overlap. The polarization can be transferred either to the ^{13}C$^{\alpha}$ or to the ^{15}N to have a single "read-out" proton. We have chosen to transfer through the ^{13}C$^{\alpha}$ to the ^{1}H$^{\alpha}$ (Fig. 1**a, 3a**) to avoid disturbing any stored ^{15}N polarization, and because we have sufficient resolution in this sample at this spinning rate. This results in an hC'cαHα experiment, where the 2D correlation spectrum encodes the i^{th} residue ^{13}C' and ^{1}H$^{\alpha}$ frequency. The transfer efficiency of the COSY [41] scheme used for ^{13}C–^{13}C polarization transfer is similar to, or better than, a ^{13}C–^{15}N transfer and is much easier to set up experimentally. While we chose COSY mixing for ease of use, any number of other homonuclear mixing schemes could be used.

To adapt the individual experiments into simultaneous experiments the initial excitation period is turned into a SIM-CP period so that both pathways are excited. We then must identify the longest-lived state and store this state after the SIM-CP excitation. The experiment is acquired on the short-lived state(s) first. Then, the stored polarization is re-excited, and an experiment is acquired on the long-lived state with a second, separate acquisition. This approach should mitigate losses from relaxation and simplifies the timings and polarization transfers that would be needed for a single acquisition of multiple pathways.

Simultaneous measurement of ^{13}C' and ^{15}N R_1

The ^{13}C' (hC'cαH) and ^{15}N (hNH) R_1 measurements (Fig. 1**a** and 1**b** respectively) can be combined relatively straightforwardly

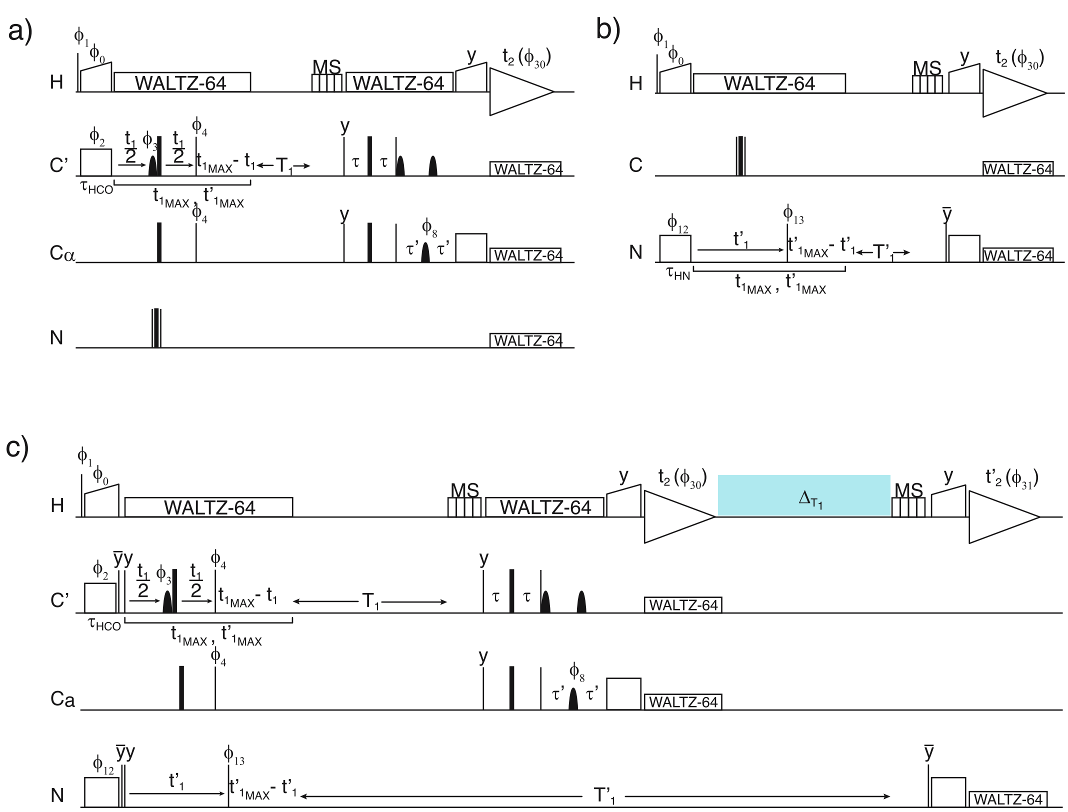

Fig. 1. Pulse sequence of individual a) hC'cαHα R_1 and b) hNH R_1 measurement, and c) combination in the staggered acquisition experiment. Narrow and broad black lines represent 90° and 180° hard pulses, respectively. Rounded pulses represent 180° selective shaped pulses. When not shown, the phase of the pulses is x. The phase cycling for both the experiments is as follow: φ_0= {y*8, -y*8}, φ_1= {x*2, -x*2}, φ_2= {x*16, -x*16}, φ_3= {y*4, x*4}, φ_4= {-y, y}, φ_8= {x*32, y*32} and acquisition φ_{30}= {y, -y, -y, y, -y, y, y, -y, -y, y, y, -y, y, -y, -y, y, -y, y, y, -y, y, -y, -y, y, y, -y, -y, y, -y, y, y, -y, -y, y, y, -y, y, -y, -y, y, y, -y, -y, y, -y, y, y, -y, y, -y, -y, y, -y, y, y, -y, -y, y, y, -y, y, -y, -y, y}for the hC'CαHα portion. φ_{12}= {x*2, -x*2}, φ_{13}= {y, -y}, φ_{16}= {x*4, -x*4} and acquisition φ_{31}= {-y, y, y, -y, y, -y, -y, y, y, -y, -y, y, -y, y, y, -y} for the hNH portion. States-TPPI is employed on φ_4 (**a**, **c**) and φ_{13} (**b**, **c**).

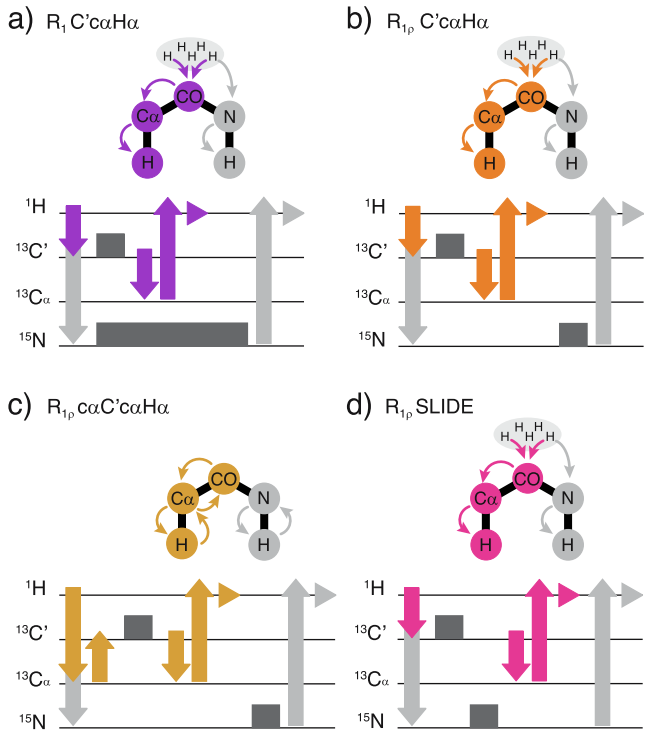

Fig. 2. Schematic representation of ^{13}C (colour specified in each implementation) and ^{15}N (light grey) magnetization pathway for the a) staggered R_1 hC'cαHα + hNH_N (violet) implementation and staggered $R_{1\rho}$ measurements b) hC'cαHα + hNH_N (orange), c) hcαC'cαHα + hNH_N (gold) and d) SLIDE (pink) experiments. $R_{1\rho}$ and R_1 times are represented by dark grey blocks. (For interpretation of the references to colour in this figure legend, the reader is referred to the web version of this article.)

(Fig. 1**c**). A schematic representation of the magnetization pathways is found in Fig. 2**a**. The individual pseudo-3D alters the 2D correlation experiment by adding a relaxation delay after the chemical shift encoding and immediately before the water suppression (we choose simultaneous rather than sequential relaxation periods to avoid large increases in experimental times due to required long relaxation delays). It is not strictly necessary to encode the chemical shift before the relaxation period. Indeed, the resolution could be better for $^{13}C^{\alpha}$ rather than $^{13}C'$, however $^{13}C'$ was labelled to prove the desired polarization pathway was achieved. Alternative schemes for the ^{13}C homonuclear transfer and chemical shift labelling may be more efficient than this implementation [42]. To combine the two experiments, the initial CP is converted to simultaneous cross-polarization (SIM-CP), and then the ^{15}N and $^{13}C'$ chemical shift is encoded simultaneously (time-shared). Once the longest of the chemical shift delays is finished, the clock for both T_1 delays starts. The delays required to sample the relaxation times of each nucleus are on the same order of magnitude, but the $^{13}C'$ relaxation time is approximately half of the ^{15}N relaxation time. The $^{13}C'$ experiment is thus finished relaxing well before the ^{15}N. Therefore, the $^{13}C'$ pathway is acquired while the ^{15}N is still relaxing. This has the consequence that the ^{15}N delay has to be sufficiently long to allow the $^{13}C'$ pathway experiment to finish, which includes the $^{13}C'$ relaxation delay time, homonuclear transfer, and the acquisition on $^{1}H^{\alpha}$.

To ensure appropriate alignment of the two polarisation transfer pathways, the remainder of the ^{15}N delay (Δ_{T1}) is calculated as shown by equation (1.1).

$$\Delta_{T_1} = T_1' - (T_1 + MS + {}^{13}C^{1}H\,CP + COSY + t_2) \tag{1.1}$$

The duration of the solvent suppression (MS), COSY transfer, $^{13}C^{\alpha}$–$^{1}H^{\alpha}$ CP and acquisition is on the scale of 100 ms, so the first point of the ^{15}N relaxation time must be longer than this time. A long initial time delay is only relevant when fast relaxing ^{15}Ns are present in the sample but is not much of a concern in general. For example, if the initial time point is 100 ms the signal would be lost for an ^{15}N with a T_1 < 30 ms, but typical backbone ^{15}N T_1s are on the order of dozens of seconds. ^{1}H–$^{15}N/^{13}C'$ cross-correlation effects are thought to be negligible due to self-decoupling effects [43,44]. To ensure that cross-correlated relaxation effects are completely supressed a series of π-pulses on the ^{1}H channel could be applied [45] (and easily incorporated into our sequences) but in our hands such procedure made no difference for fully protonated GB1 at 100 kHz spinning [29]. Consequently, since there is no requirement for any complex irradiation schemes during the relaxation delay, there is no need for separate relaxation delays for the two types of nuclei. The $^{13}C'$ experiment is effectively collected during the ^{15}N experiment, which means that the overall pulse sequence duration is equal to the standard ^{15}N R_1 experiment. Thus, with the same overall experimental time of a ^{15}N R_1 experiment we also obtain a $^{13}C'$ R_1 measurement. The same concept can be applied for aliphatic carbons ($^{13}C^{ali}$) on the peptide side chain in an alternately ^{13}C-labelled sample (i.e. samples expressed using (1,3) or (2) ^{13}C glycerol, (1) or (2) ^{13}C glucose, or other such labelling schemes).

Fig. 3**a** and 3**b** show the 2D $^{1}H^{\alpha}$–$^{13}C'$ and ^{1}H–^{15}N 2D GB1 correlation spectra from the first slice of the staggered hC'cαHα + hNH_N experiment. Fig. 3**b** is a typical 2D ^{1}H–^{15}N fingerprint GB1 spectrum, while Fig. 3**a** is the 2D hC'cαHα correlation with 60 observable peaks, considering two $^{1}H^{\alpha}$ for each glycine. The latter spectrum is detected on $^{1}H^{\alpha}$, which is possible due to the good spectral resolution at 100 kHz spinning frequency [46,47] and the efficient water suppression from the MISSISSIPPI scheme [34]. The sensitivity of the hC'cαHα spectrum is ~ 80% the hNH_N spectrum principally due to signal lost during the C' to C^{α} COSY transfer. The signal derived from the $^{13}C'$ of glycine residues is transferred to both of the $^{1}H^{\alpha}$ protons, resulting in a lower relative signal intensity. The individual relaxation rates extracted from one consistent $^{1}H^{\alpha}$–$^{13}C'$ glycine peak is fitted and reported.

The final point of concern is whether the application of pulses on the ^{13}C and ^{1}H channels during the ^{15}N R_1 relaxation delay interferes with the measurement itself. However, since the $^{13}C'$ and ^{15}N R_1 rates found using the single and combined experiments are the same within error (Fig. 3**c,d**) we conclude that any interference effects are here negligible.

Simultaneous measurement of ^{15}N and $^{13}C'$ $R_{1\rho}$

The individual $^{13}C'$ and ^{15}N $R_{1\rho}$ experiments are adapted for ^{1}H-detection by adding a spinlock into correlation experiments that were used in the previous section, as shown in Fig. 4**a,b**. Since ^{15}N is expected to have the greater $T_{1\rho}$, and there is only an inversion during the ^{13}C experiment, we perform the ^{13}C-based transient of the experiments first, and then do the ^{15}N-based transient (Fig. 4**c**). To be more specific, in the first multiple pathway variant (Fig. 2**b**) the magnetization is transferred from ^{1}H to $^{13}C'$ and ^{15}N, generating two polarization paths from the "bulk" ^{1}H polarization. SIM-CP for $^{13}C'$ and ^{15}N may draw from the same pool of polarization so the $^{13}C'$ might leech polarization from the ^{15}N, or vice versa. To prevent dilution of the initial polarization pool, a pathway (Fig. 2**c**) was devised where the polarization is transferred from the $^{1}H^{\alpha}$ to the $^{13}C^{\alpha}$, and from $^{1}H^{N}$ to ^{15}N using short duration, one-bond transfers, so specific ^{1}H polarization pools are utilized. An experiment was then constructed to chauffeur the polarization from $^{1}H^{\alpha}$ to $^{13}C^{\alpha}$ to $^{13}C'$, and then back (Fig. 4**d**). The source of the polarization should, thus, be different

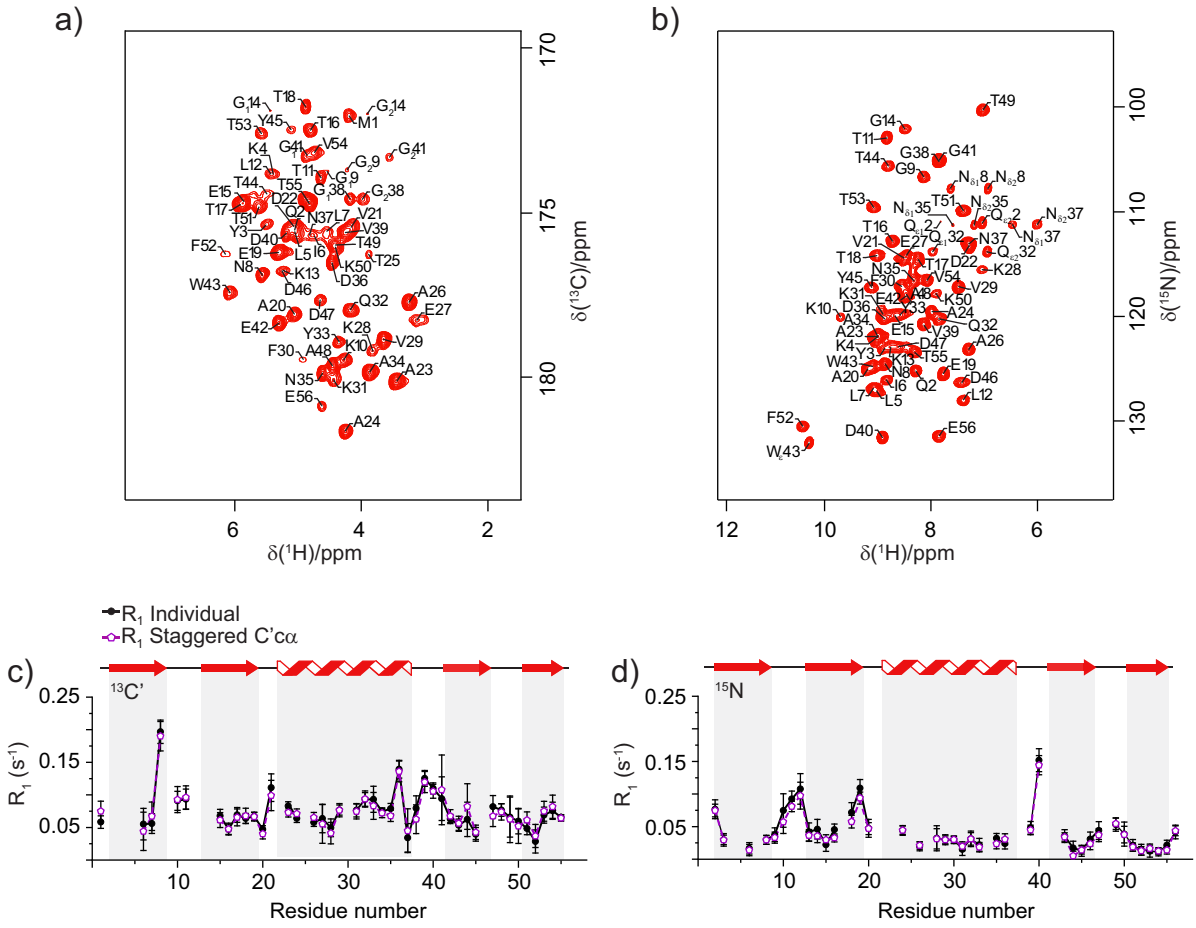

Fig. 3. 2D spectra for crystalline [U-^{13}C,^{15}N]GB1 obtained at 100 kHz spinning with assignments: a) hC′cαHα and b) N-H_N. Comparison of c) ^{13}C′ and d) ^{15}N R_1 rates per residue between the standard hC′cαHα and hNH$_N$ experiments (blue) and staggered acquisition (violet). Error bars represent two standard deviations within the correspondent rate. For the severely overlapping peaks, values were removed. (For interpretation of the references to colour in this figure legend, the reader is referred to the web version of this article.)

for ^{13}C' and ^{15}N, which could improve the initial CP efficiency enough to compensate for the extra transfers. In both experiments, after the SIM-CP, the ^{15}N polarization is stored while the spin-gymnastics are happening on the ^{13}C channel. The experiments are the same after the COSY transfer to ^{13}C'. The $R_{1\rho}$ spinlock is applied on the ^{13}C', followed by ^{13}C' chemical shift evolution. The ^{13}C' coherence is then transferred to $^{13}C^{\alpha}$ through COSY transfer and the signal acquired on $^{1}H^{\alpha}$ after $^{13}C^{\alpha}$–$^{1}H^{\alpha}$ CP. A waiting period is inserted after the first detection period so the ^{15}N measurement starts at a constant time after excitation to avoid any T_1(^{15}N) contribution to the observed rate. The ^{15}N and ^{13}C' spinlocking fields are implemented sequentially rather than simultaneously to avoid any potential interference or recoupling effects between ^{15}N and ^{13}C pulses. The ^{15}N magnetization is then re-excited to encode the ^{15}N $R_{1\rho}$ and ^{15}N chemical shift, and the signal is acquired on $^{1}H^{N}$ after ^{15}N–^{1}H CP. ^{15}N decoupling is turned off during the $^{1}H^{\alpha}$ acquisition to preserve the stored polarization; its application has a negligible effect on the $^{1}H^{\alpha}$ linewidth. ^{13}C decoupling is applied during all acquisition periods, even though there is little effect on the H^{N} resonance, because the ^{13}C polarization was detected previously, and thus it is not important to preserve. A soft-hard π-pulse pair is used during chemical shift evolution to ensure that the proper ^{13}C pathway is selected; the removal of the homonuclear scalar coupling is a secondary bonus of this approach.

The ^{15}N read-out portion is delayed by:

$$\Delta = T_{1\rho MAX} - T_{1\rho(n)} + 10ms \quad (1.2)$$

where $T_{1\rho MAX}$ is the longest spinlocking pulse that will be used in the experiment, $T_{1\rho(n)}$ is the current spinlocking pulse time, and 10 ms is arbitrarily added to avoid negative times. If detuning or heating from the ^{13}C spinlocking pulse are a concern, the spinlock field could be turned on during this waiting period. In the context of presented here experiments, removing Δ altogether would reduce the experiment time by ~ 1 h compared to 10 h total time but might introduce variation from ^{15}N longitudinal relaxation.

Fig. 5**a-d** shows the comparison of the measured site-specific ^{13}C' and ^{15}N $R_{1\rho}$ rates for the individual/singleton and the staggered hC′cαHα + hNH$_N$ and hcαC′cαHα + hNH$_N$ implementations of the experiment. The sensitivity of the hC′cαHα spectrum is ~ 60% of the HN spectrum principally due to signal lost during the ^{13}C' to $^{13}C^{\alpha}$ COSY transfer. The sensitivity of the hcαC′cαHα spectrum is ~ 40% of the HN spectrum, which indicates that selecting the polarization pool did not compensate for the polarization lost during the transfer; the direct ^{1}H–^{13}C' CP version is more efficient. The measured rates for all comparable experiments are the same within the experimental error. This demonstrates that the measured ^{13}C' and ^{15}N $R_{1\rho}$ relaxation rates are not affected by additional pulses used during the staggered experiments. The results are the same as the individual experiments, but more data is acquired for a given experimental time. The comparison of the relaxation curves measured using the standard experiments with

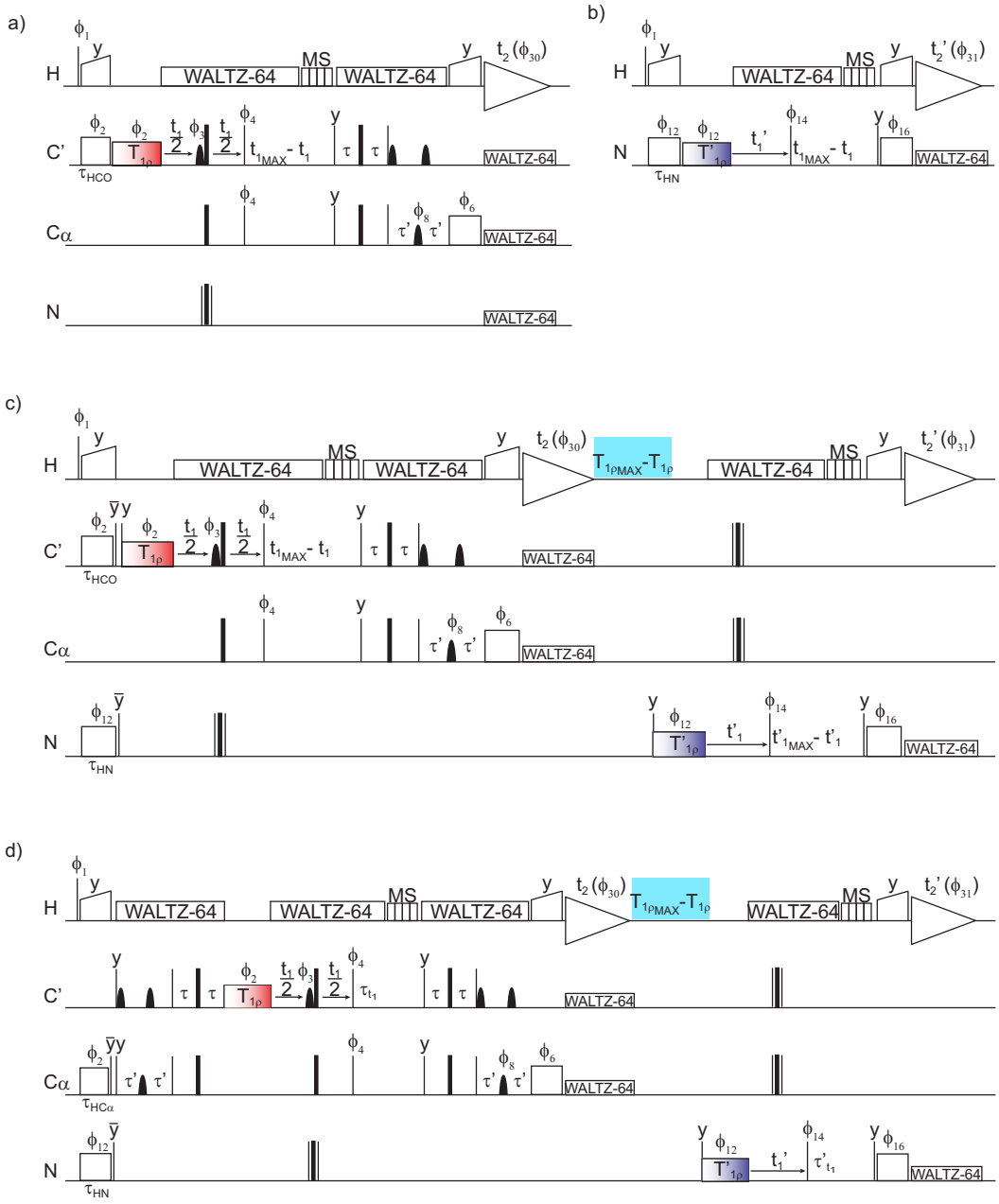

Fig. 4. Pulse sequence of individual a) hC′cαHα ^{13}C′ $R_{1\rho}$, b) hNH$_N$ ^{15}N $R_{1\rho}$ experiment, Staggered acquisition c) hC′cαHα + hNH$_N$ (C′+N) $R_{1\rho}$ and d) hcαC′cαHα + hNH$_N$ (C′+N) $R_{1\rho}$, where τ_{t1} = t_{1MAX}-$t_1$and τ'_{t1} = t'_{1MAX}-t'_1 Narrow and broad black lines represent 90° and 180° hard pulses, respectively. Rounded pulses represent 180° selective shaped pulses. When not shown, the phase of the pulses is x. The phase cycling for both the experiments is as follow: φ_1= {x*8, -x*8}, φ_2= {x*2, -x*2}, φ_3= {y*4, x*4}, φ_4= {-y, y}, φ_6= {x*16, -x*16}, φ_8= {x*32, y*32} and acquisition φ_{30}= {y, -y, -y, y, -y, y, y, -y, -y, y, y, -y, y, -y, -y, y, y, -y, y, -y, -y, y, y, -y, -y, y, -y, y, y, -y, -y, y, y, -y, -y, y, -y, y, -y, y, y, -y, -y, y, -y, y, y, -y, y, -y, -y, y}for the hC'cαHα portion. φ_{12}= {x*2, -x*2}, φ_{14}= {y, -y}, φ_{16}= {x*4, -x*4} and acquisition φ_{31}= {-y, y, y, -y, y, -y, -y, y, y, -y, -y, y, -y, y, y, -y} for the hNH$_N$ portion. States-TPPI is employed on φ_4 (**a**, **c**, **d**) and φ_{14} (**b**, **c**, **d**).

the multiple acquisition experiments presented here can be found in the Supporting Information.

To reduce the experiment time further, the chemical shift and spinlock periods can be optimized with time-sharing. The chemical shift is allowed to evolve on the two nuclei, ^{13}C' (t_1) and ^{15}N (t'_1) at the same time (Fig. 6**a**). The evolution time is implemented so that the polarization for both nuclei is stored for the longest of the two nested evolutions t_1 and t'_1. To avoid unintended magnetization transfers or any other interference during the spinlock, (*e.g.* CP), the spinlocks are never applied at the same time. The spinlock pulses are combined by **S**imultaneous**Ly** **I**ncreasing and **DE**creasing (SLIDE) the times, where the ^{13}C time increments but the ^{15}N decrements to fit the experiments in a constant time period (Fig. 6**b**). This SLIDE period is constructed by inserting the delay Δ_{SLIDE} between the two spinlock periods to limit the contribution from T_1 and to separate the spinlock pulses on the two nuclei. The delay Δ_{SLIDE}, is described by:

$$\Delta_{SLIDE} = T_{1\rho MAX} + T'_{1\rho MAX} - (T_{1\rho} + T'_{1\rho}) + 10ms \quad (1.3)$$

These modifications reduce the experiment time by 1 h from the staggered experiment, for a total of 9 h acquisition, a total savings of 40% with respect to the two individual experiments (15 h in total). If sample heating during the spinlock periods is a concern, compensatory pulses can be added either before the initial excitation or after the final acquisition.

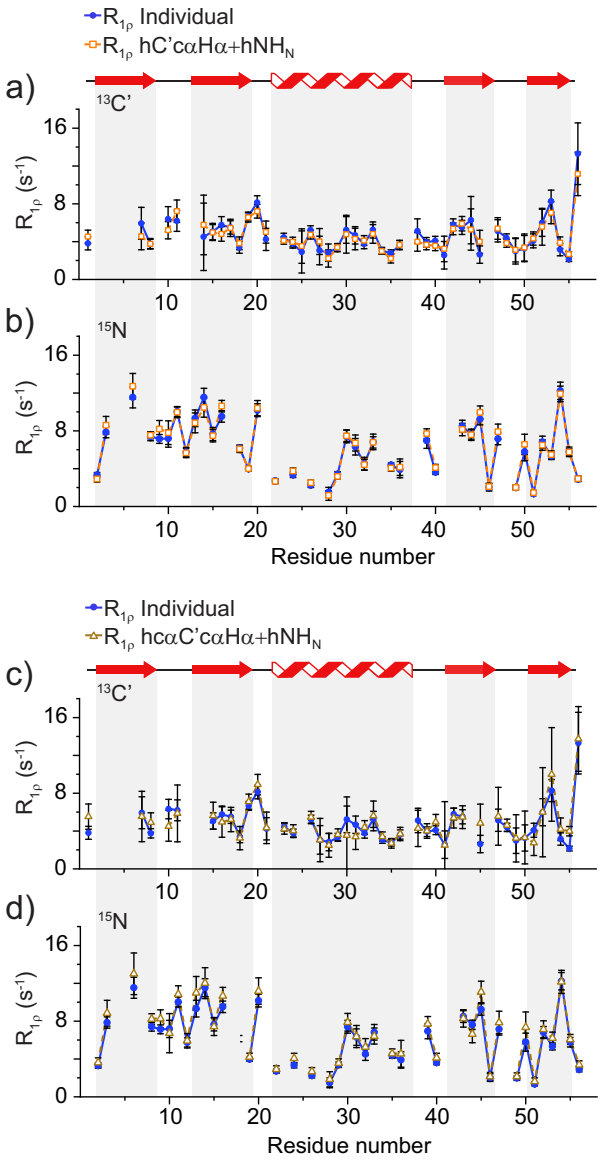

Fig. 5. A comparison of the $R_{1\rho}$ rates for a) ^{13}C' and b) ^{15}N between the separate single-acquisition experiments (blue) and staggered hC'cαHα + hNH$_N$ (orange- empty square) double acquisition experiments as a function of the residue number. Comparison of $R_{1\rho}$ rates of c) ^{13}C' and d) ^{15}N between the separate single-acquisition experiment (blue) and staggered hcαC'cαHα + hNH$_N$ (gold- empty triangle) double acquisition experiments. Error bars represent two standard deviations within the correspondent rate. For the severely overlapping peaks values are not included. (For interpretation of the references to colour in this figure legend, the reader is referred to the web version of this article.)

A concern with the SLIDE experiment is the introduction of changes in the peak intensity due to T_1 relaxation into the $T_{1\rho}$ data. For crystalline GB1 this is not a large concern since the $T_{1\rho}$ of ^{15}N and ^{13}C' are an order of magnitude shorter than T_1, and thus the differences in the intensity due to T_1 relaxation are smaller than the overall experimental error. If T_1s were shorter, the use of constant time periods throughout the experiment will negate any T_1 effects.

Since the ^{15}N pulse does not always start at the same time, the T_1 relaxation could have an effect on the measured $R_{1\rho}$ rates. However, in our case this is negligible because the longest time wait on ^{15}N, 210 ms (Δ + T_1(^{13}C'), for the last time-point delay) should result in the intensity changes < 2%. This is demonstrated in the comparison of the resulting $R_{1\rho}$ rates between SLIDE and the individual hC'cαHα and hNH$_N$ experiments, which are the same within error (Fig. 6**c,d**), and in the sensitivity of SIM-CP (see below).

As a comparison between SLIDE and the other staggered $R_{1\rho}$ variants, the delay Δ in the hC'cαHα + hNH$_N$ and hcαC'cαHα + h NH$_N$ experiments, an additional time waiting with respect to SLIDE, is not required and could be eliminated, since T_1 effects do not introduce a large error in the $R_{1\rho}$ rates measurements. This would save one hour in our reference experiment, calculated with the sum of Δ for each FID, making hC'cαHα + hNH$_N$ last as long as SLIDE. This statement is valid for GB1, which has long relaxation times, but for other bio-macromolecules, typically with shorter T_1s, Δ becomes fundamental to assure that the longitudinal relaxation does not compromise the ^{15}N $R_{1\rho}$ data, where the ^{15}N experiment always has the same starting point relative to the initial excitation.

Sensitivity and Time Savings

To get a better idea of time savings achievable with staggered experiments, we compare the staggered experiments time with the singleton experiments run sequentially. If there were no losses in sensitivity between standard and SIM-CP and there were no differences in relaxation delay schedules, staggered experiments could produce a maximum factor of 2 in time saving. However, SIM-CP is typically slightly less sensitive than standard CP (i.e. individual ^{1}H-^{15}N and ^{1}H–^{13}C) meaning that more transients need to be acquired to obtain the same signal-to-noise ratio (SNR) in the staggered experiments compared to equivalent singleton experiments. In the first instance, we have used SIM-CP settings obtained from optimisation of individual CPs. In this case, we observed that we lose 12% and 8% efficiency when employing SIM-CP in R_1 measurements rather than individual ^{1}H–^{13}C' and ^{1}H-^{15}N CP steps, respectively (see Fig. 7). For the $R_{1\rho}$ measurements with the favourable hC'cαHα + hNH$_N$ pathway the observed decreases in efficiency are 15 and 10% for the staggered ^{13}C' and ^{15}N relaxation measurements (see Fig. 8). This means that by accounting for the additional transients that need to be acquired to get the same SNR as in individual experiments the staggered experiments time saving factors would be reduced from the theoretical maximum of 2 to ~ 1.6 for R_1 and ~ 1.5 for $R_{1\rho}$.

We have investigated whether the SIM-CP losses can be minimised if the optimisation is performed directly on the SIM-CP experiment instead of transferring the settings from optimisations for individual CPs. Indeed, if SIM-CP is optimised directly on crystalline GB1 the losses compared to individual CPs can be reduced. Fig. 8 shows comparisons between first points for singleton and staggered $R_{1\rho}$ experiments where SIM-CP was optimised directly rather than using settings from individual CPs. We can see that for the preferential hC'cαHα + hNH$_N$ pathway the SIM-CP losses are reduced to 12 and 3% for ^{13}C' and ^{15}N relaxation measurements. This means that in theory we could get ~ 1.7 times saving from employing staggered $R_{1\rho}$ and, by extrapolation, up to ~ 1.76 times from staggered R_1 experiments.

For a completely fair comparison of time savings between singleton and staggered experiments we also have to: 1. take into account that one may choose different relaxation delay schedules for these experiments and 2. account for differences in pulse sequence duration in the case of sequential experiments.

For backbone R_1 measurements, relaxation delays much longer than the recycle delay are often required and a few experiments with the longest relaxation delays dominate the overall experimental time. In the case of singleton experiments, the relaxation delays can be tailored to individual relaxation probes with longer final delays for the nuclei with longer T_1s and shorter final delays for nuclei with shorter T_1s. In the case of staggered experiments, the longest relaxation delays will be dictated by the slower

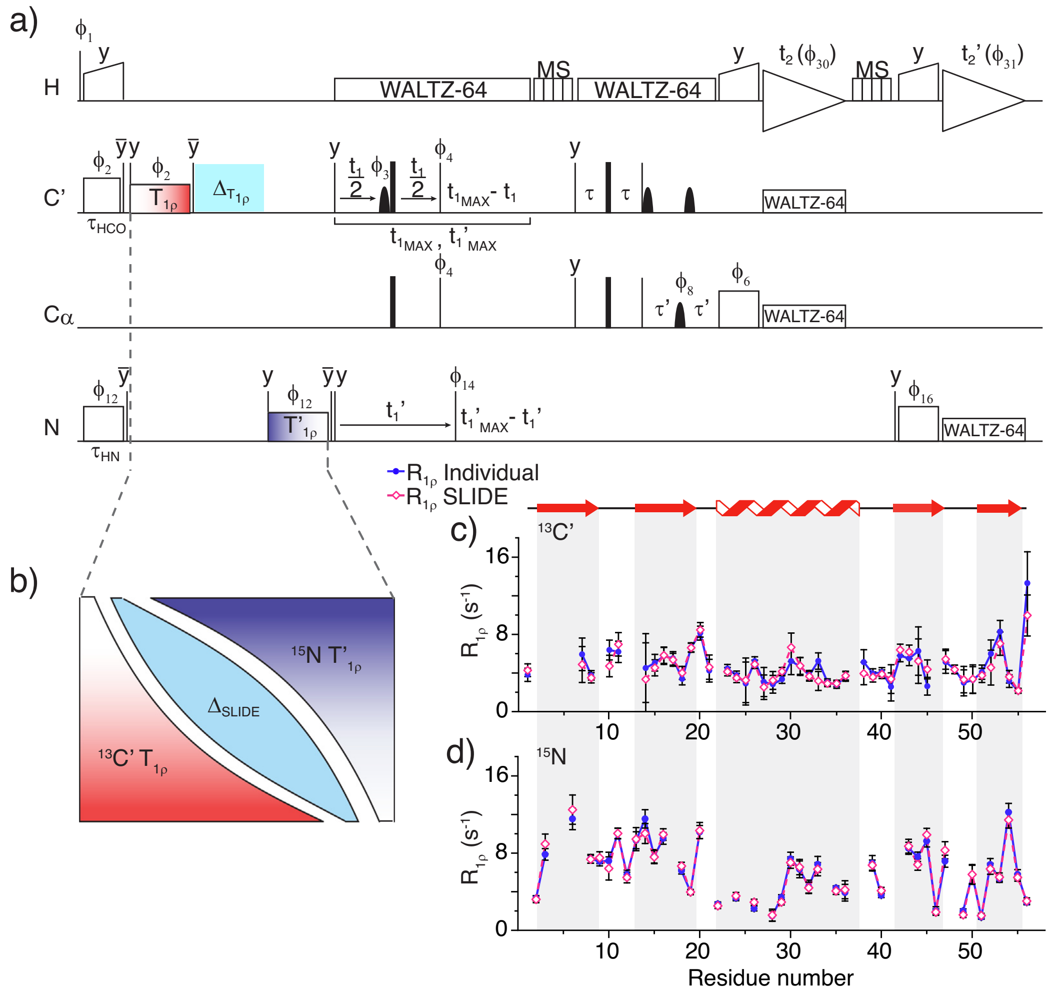

Fig. 6. Time share a) pulse sequence with b) zoom of the constant time defined by ^{13}C' incrementing, ^{15}N decrementing $T_{1\rho}$ lists and $\Delta_{T1\rho}$. Comparison of c) ^{13}C' and d) ^{15}N $R_{1\rho}$ rates per residue between the standard hC'cαHα and hNH$_N$ experiments (blue) and SLIDE (pink). Error bars represent two standard deviations within the correspondent rate. For the severely overlapping peaks, values were removed. Narrow and broad black lines represent 90° and 180° hard pulses, respectively. Rounded pulses represent 180° selective shaped pulses. When not shown, the phase of the pulses is x. The phase cycling for both the experiments is as follow: φ_1= {x*8, -x*8}, φ_2= {x*2, -x*2}, φ_3= {y*4, x*4}, φ_4= {-y, y}, φ_6= {x*16, -x*16}, φ_8= {x*32, y*32} and acquisition φ_{30}= {y, -y, -y, y, -y, y, y, -y, -y, y, y, -y, y, -y, -y, y, -y, y, y, -y, y, -y, -y, y, y, -y, -y, y, -y, y, y, -y, -y, y, y, -y, y, -y, -y, y, y, -y, -y, y, -y, y, y, -y, y, -y, -y, y, -y, y, y, -y, -y, y, y, -y, y, -y, -y, y} for the hC'cαHα portion. φ_{12}= {x*2, -x*2}, φ_{14}= {y, -y}, φ_{16}= {x*4, -x*4} and acquisition φ_{31}= {-y, y, y, -y, y, -y, -y, y, y, -y, -y, y, -y, y, y, -y} for the hNH$_N$ portion. States-TPPI is employed on φ_4 and φ_{14} in **a**. (For interpretation of the references to colour in this figure legend, the reader is referred to the web version of this article.)

relaxing nucleus: typically, ^{15}N. In $R_{1\rho}$ measurements where the relaxation times are typically shorter than the recycle delay, the choice of the longest delays has a less dramatic effect on the overall experimental time.

For the staggered acquisition R_1 measurements, the ^{13}C' sampling schedule is built into the ^{15}N schedule, so the staggered experiments have the same length as the ^{15}N individual experiments. In this context, the saved time from staggered implementation corresponds to the duration of the ^{13}C' experiments: ^{13}C' experiment takes place during the ^{15}N R_1 measurements and the relaxation delay is shared. However, if ^{13}C' T_1s are significantly shorter than ^{15}N T_1s the longest relaxation delays in singleton ^{13}C' experiments can be shorter than the relaxation delays dictated by ^{15}N T_1s in a staggered experiment.

Comparisons can get very quickly complicated depending on precise choice of sampling and experimental conditions. Consequently, below we discuss one illustrative example in order to highlight general considerations for running staggered vs. singleton experiments rather than provide absolute numbers.

At 700 MHz spectrometer in crystalline GB1 at room temperature the average ^{15}N and ^{13}C' T_1s are on the order of 25 and 12.5 s respectively. If we chose to sample the relaxation delays up to 1x T_1, this means that the longest delays would be 25 s for ^{15}N and 12.5 s for ^{13}C'. If we use seven logarithmically spaced sampling of relaxation delays from 0.2 to 25 s in case of ^{15}N and 0.2 to 12.5 s in case of ^{13}C', we get 0.20, 0.45, 1.00, 2.24, 5.00, 11.18, 25.00 sampling for ^{15}N and 0.20, 0.40, 0.79, 1.58, 3.1498, 6.27, 12.50 sampling schedule for ^{13}C'. Taking these sampling schedules and the experimental parameters we used on GB1, the individual ^{15}N R_1 measurement would take approximately 27 h and individual ^{13}C' R_1 measurement about 14.7 h. If we chose the ^{15}N schedule for the staggered R_1 measurement it would take ~ 27 h. This means that if there is no difference in sensitivity, the staggered experiment would take ~ 1.55 times shorter rather than 2 times shorter. Considering the decreases in sensitivity due to lower efficiency of SIM-CP we discussed above, the real time saving factor for running staggered R_1 measurement would be ~ 1.4 times.

It is important to point out that in the above comparison the main difference comes from the experiments with the longest relaxation delays. In the example discussed above the last 2D with relaxation delay of 25 s would take ~ 14.3 h, which is more than all the other six points in this experiment or almost as long as all 7

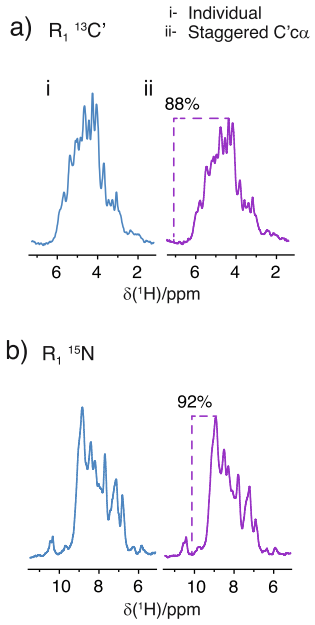

Fig. 7. Sensitivity comparison of ^{1}H 1D integrated spectrum intensity on a) ^{13}C' and b) ^{15}N for the R_1 individual experiments with initial ^{1}H–^{13}C and ^{1}H-^{15}N CP steps (i) and staggered acquisition experiment with initial ^{1}H-^{15}N/^{13}C CP step (ii). The ^{1}H 1D integrated spectrum intensity of the staggered acquisition is indicated as a percentage scaled to the individual experiment (100%). The experiments were acquired consecutively with 512 coadded transients. In this case SIM-CP settings were based on the settings optimised on individual ^{1}H-^{15}N and ^{1}H–^{13}C CP steps.

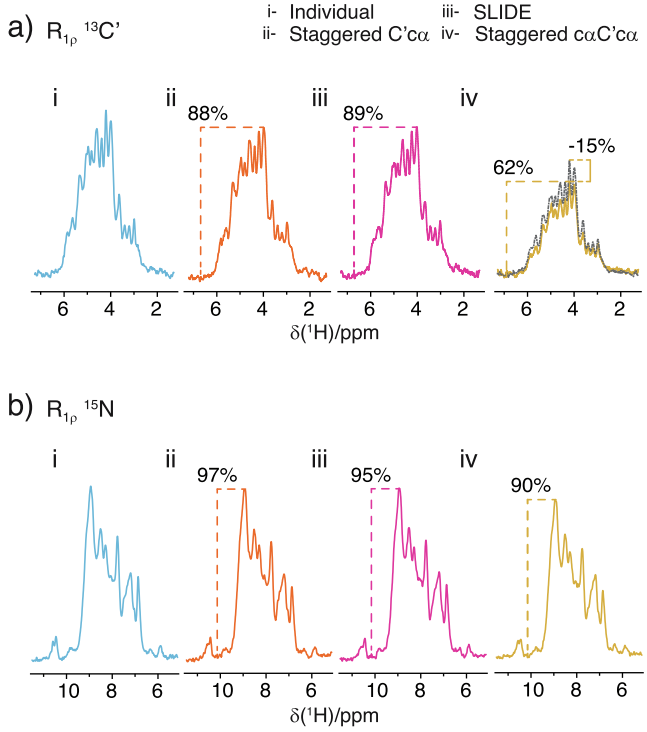

Fig. 8. Sensitivity comparison of ^{1}H 1D integrated spectrum intensity on a) ^{13}C' and b) ^{15}N for the $R_{1\rho}$ individual experiment (i, blue), staggered hC'cαHα + hNH$_N$ (ii, orange), SLIDE (iii, pink) and hcαC'cαHα + hNH$_N$ (iv, gold). The individual hcαC'cαHα intensity is shown in (a, iv) in dotted line on gold solid line and the SIM-CP is 15% lower than the individual experiment. The ^{1}H 1D integrated spectrum intensity of each staggered acquisitions is indicated as a percentage scaled to the individual experiment (100%). (For interpretation of the references to colour in this figure legend, the reader is referred to the web version of this article.)

points in the individual ^{13}C R_1 measurement (14.7 h). This highlights that the percentage time gain from using a staggered experiment will be better the closer to each other the maximum relaxation delays for ^{13}C and ^{15}N experiments are, and that for more dynamic samples with shorter relaxation times (i.e. more challenging samples) the percentage gains will improve as well. Notably for $R_{1\rho}$ measurements where relaxation delays are typically shorter than recycle delay, the impact of the different sampling schedules in the individual vs. staggered experiments will be much smaller than for R_1 measurements.

Overall, one could expect 1.3–1.6 times real saving in time by using staggered experiments for measuring ^{15}N and ^{13}C' R_1 and $R_{1\rho}$ relaxation. Even though these savings might not appear very large as percentage gain, because relaxation measurements can be really time consuming, real time savings may be very respectable in absolute terms when applied to challenging samples. For example, measurement of ^{15}N R_1 on GB1:IgG complex requires about two–three weeks of experimental time and most likely comparable amount of time for ^{13}C' R_1 measurements. In this particular case, staggered experiments would result in real time savings of about two weeks compared to individual experiments.

4. Conclusion

In summary, we propose approaches for simultaneous acquisition of ^{15}N and ^{13}C R_1 and $R_{1\rho}$ using ^{1}H-detected experiments at fast (100 kHz) spinning on fully protonated protein samples. We employ sequential ^{15}N and ^{13}C acquisition with concurrent relaxation delay periods for R_1 and sequential ^{15}N and ^{13}C spinlocking pulses for $R_{1\rho}$ measurements. The ^{15}N experiments are detected on amide ^{1}Hs and ^{13}C' experiments are detected on ^{1}H$^{\alpha}$s. For ^{13}C' experiments we find that hC'cαHα pathway yields higher SNR compared to hcαC'cαHα pathway. We propose various solutions to further minimise the overall experimental time through, *e.g.* time-shared evolution or SLIDE for time-optimised sampling of ^{15}N and ^{13}C spinlocking pulses (all pulse sequences in Bruker format are available for download from: http://dx.https://doi.org/10.17632/x7kk4rkpj3.1.). The relaxation rates obtained from simultaneous experiments are within experimental error the same as the relaxation rates obtained from the individual experiments. In crystalline GB1, the real time gains for simultaneous ^{15}N and ^{13}C' relaxation measurements are about 1.2–1.4 times for R_1 and 1.3–1.5 times for $R_{1\rho}$ compared to running individual experiments. Calculation of the real time gains takes into account SNR losses due to application of SIM-CP compared to conventional CP and additional delays, as well as pulse sequence duration increases due to sequential acquisition. These gains should improve further for dynamic proteins with shorter relaxation times and thus shorter required relaxation delays. The approaches demonstrated here improve the practicality of powerful but time-consuming relaxation measurements for quantifying protein dynamics in the solid-state.

This approach may be less effective with other typical sample preparation protocols, for example triply labelled and back exchanged samples. In triply labelled samples the amide protons are the only available source of polarization, so the efficiency of SIM-CP is expected to be reduced. Both experiments lose sensitivity due to sharing one polarization source, with additional loss for ^{13}C' due to the long ^{13}C'-^{1}H CP contact time that increases the number of correlations (where the ^{13}C'-^{13}C$^{\alpha}$ transfer would be removed). While the application of these experiments to samples with one polarization source does not seem promising that does not preclude its application to all deuterated samples. Our approach might be worthwhile to improve the measurement rate of sidechain relaxation in samples with high degree of deuterium

labelling. In the case of the R_1 experiments only, these results indicate that it should be possible to run other experiments while waiting on the relaxation similar to embedded experiments on materials [48].

The resolution of the spectra is another factor in the applicability of these experiments, as it is for all pseudo-3D methods. While it is not routinely done, it should be possible to adapt these experiments into pseudo-4D experiments. The 3D experiments would be combined around a common pulse sequence elements such as a CN/NC transfer in the hNCH and hCNH, and the relaxation period is added at an appropriate place before the transfer back to proton. The experiment time to acquire a series of 3Ds is likely to be prohibitively long (which is one reason they are rarely acquired), so a reduced dimensionality style experiment or sparse sampling scheme would likely need to be applied. In that same vein, the resolution of the ^{13}C spectra could probably be improved by labelling the chemical shift of the $^{13}C^{\alpha}$ nucleus or combining the $^{13}C'$ and $^{13}C^{\alpha}$ chemical shift evolution.

Declaration of Competing Interest

The authors declare that they have no known competing financial interests or personal relationships that could have appeared to influence the work reported in this paper.

Acknowledgements

The authors declare no conflicts of interest. We thank Professor Steven P. Brown for helpful discussions. The research leading to these results has received funding from the European Research Council under the European Union's Seventh Framework Programme (FP/2007-2013) / ERC Grant Agreement 639907. J.R.L. also acknowledges funding from BBSRC Grant BB/R010218/1. Jacqueline Tognetti thanks EPSRC for a PhD studentship through the EPSRC Centre for Doctoral Training in Molecular Analytical Science, grant number EP/L015307/1.

Appendix A. Supplementary material

Supplementary data to this article can be found online at https://doi.org/10.1016/j.jmr.2021.107049.

References

[1] J.M. Lamley, J.R. Lewandowski, Relaxation-based magic-angle spinning NMR approaches for studying protein dynamics, EMagRes. 5 (2016) 1423–1434. https://doi.org/10.1002/9780470034590.emrstm1417.
[2] J.M. Lamley, M.J. Lougher, H.J. Sass, M. Rogowski, S. Grzesiek, J.R. Lewandowski, Unraveling the complexity of protein backbone dynamics with combined ^{13}C and ^{15}N solid-state NMR relaxation measurements, Phys. Chem. Chem. Phys. 17 (34) (2015) 21997–22008, https://doi.org/10.1039/C5CP03484A.
[3] P. Schanda, M. Ernst, Studying dynamics by magic-angle spinning solid-state NMR spectroscopy: Principles and applications to biomolecules, Prog. Nucl. Magn. Reson. Spectrosc. 96 (2016) 1–46, https://doi.org/10.1016/j.pnmrs.2016.02.001.
[4] J.R. Lewandowski, Advances in solid-state relaxation methodology for probing site-specific protein dynamics, Acc. Chem. Res. 46 (9) (2013) 2018–2027, https://doi.org/10.1021/ar300334g.
[5] J.M. Lamley, C. Öster, R.A. Stevens, J.R. Lewandowski, Intermolecular Interactions and Protein Dynamics by Solid-State NMR Spectroscopy, Angew. Chemie Int. Ed. 54 (51) (2015) 15374–15378, https://doi.org/10.1002/anie.v54.5110.1002/anie.201509168.
[6] C. Öster, S. Kosol, J.R. Lewandowski, Quantifying Microsecond Exchange in Large Protein Complexes with Accelerated Relaxation Dispersion Experiments in the Solid State, Sci. Rep. 9 (2019) 1–11, https://doi.org/10.1038/s41598-019-47507-8.
[7] D.B. Good, S. Wang, M.E. Ward, J. Struppe, L.S. Brown, J.R. Lewandowski, V. Ladizhansky, Conformational dynamics of a seven transmembrane helical protein Anabaena Sensory Rhodopsin probed by solid-state NMR, J. Am. Chem. Soc. 136 (7) (2014) 2833–2842, https://doi.org/10.1021/ja411633w.
[8] P. Ma, J.D. Haller, J. Zajakala, P. Macek, A.C. Sivertsen, D. Willbold, J. Boisbouvier, P. Schanda, Probing transient conformational states of proteins by solid-state $R_{1\rho}$ relaxation-dispersion NMR spectroscopy, Angew. Chemie - Int. Ed. 53 (17) (2014) 4312–4317, https://doi.org/10.1002/anie.201311275.
[9] J.R. Lewandowski, M.E. Halse, M. Blackledge, L. Emsley, Direct observation of hierarchical protein dynamics, Science (80-.). 348 (2015) 578–581. https://doi.org/10.1126/science.aaa6111.
[10] B. Busi, J.R. Yarava, A. Hofstetter, N. Salvi, D. Cala-De Paepe, J.R. Lewandowski, M. Blackledge, L. Emsley, Probing Protein Dynamics Using Multifield Variable Temperature NMR Relaxation and Molecular Dynamics Simulation, J. Phys. Chem. B. 122 (42) (2018) 9697–9702, https://doi.org/10.1021/acs.jpcb.8b0857810.1021/acs.jpcb.8b08578.s001.
[11] R. Linser, V. Chevelkov, A. Diehl, B. Reif, Sensitivity enhancement using paramagnetic relaxation in MAS solid-state NMR of perdeuterated proteins, J. Magn. Reson. 189 (2) (2007) 209–216, https://doi.org/10.1016/j.jmr.2007.09.007.
[12] N.P. Wickramasinghe, M. Kotecha, A. Samoson, J. Past, Y. Ishii, Sensitivity enhancement in ^{13}C solid-state NMR of protein microcrystals by use of paramagnetic metal ions for optimizing ^{1}H T_1 relaxation, J. Magn. Reson. 184 (2) (2007) 350–356, https://doi.org/10.1016/j.jmr.2006.10.012.
[13] S. Parthasarathy, Y. Nishiyama, Y. Ishii, Sensitivity and resolution enhanced solid-state NMR for paramagnetic systems and biomolecules under very fast magic angle spinning, Acc. Chem. Res. 46 (9) (2013) 2127–2135, https://doi.org/10.1021/ar4000482.
[14] G. Pintacuda, N. Giraud, R. Pierattelli, A. Böckmann, I. Bertini, L. Emsley, Solid-state NMR spectroscopy of a paramagnetic protein: Assignment and study of human dimeric oxidized CuII-ZnII superoxide dismutase (SOD), Angew. Chemie - Int. Ed. 46 (7) (2007) 1079–1082, https://doi.org/10.1002/(ISSN)1521-377310.1002/anie.v46:710.1002/anie.200603093.
[15] C. Öster, S. Kosol, C. Hartlmüller, J.M. Lamley, D. Iuga, A. Oss, M.-L. Org, K. Vanatalu, A. Samoson, T. Madl, J.R. Lewandowski, Characterization of Protein-Protein Interfaces in Large Complexes by Solid-State NMR Solvent Paramagnetic Relaxation Enhancements, J. Am. Chem. Soc. 139 (35) (2017) 12165–12174, https://doi.org/10.1021/jacs.7b0387510.1021/jacs.7b03875.s001.
[16] E. Lescop, T. Kern, B. Brutscher, Guidelines for the use of band-selective radiofrequency pulses in hetero-nuclear NMR: Example of longitudinal-relaxation-enhanced BEST-type ^{1}H–^{15}N correlation experiments, J. Magn. Reson. 203 (1) (2010) 190–198, https://doi.org/10.1016/j.jmr.2009.12.001.
[17] P. Schanda, V. Forge, B. Brutscher, HET-SOFAST NMR for fast detection of structural compactness and heterogeneity along polypeptide chains, Magn. Reson. Chem. 44 (S1) (2006) S177–S184, https://doi.org/10.1002/(ISSN)1097-458X10.1002/mrc.v44:1+10.1002/mrc.1825.
[18] J.M. Lamley, J.R. Lewandowski, Simultaneous acquisition of homonuclear and heteronuclear long-distance contacts with time-shared third spin assisted recoupling, J. Magn. Reson. 218 (2012) 30–34, https://doi.org/10.1016/j.jmr.2012.03.013.
[19] F. Löhr, A. Laguerre, C. Bock, S. Reckel, P.J. Connolly, N. Abdul-Manan, F. Tumulka, R. Abele, J.M. Moore, V. Dötsch, Time-shared experiments for efficient assignment of triple-selectively labeled proteins, J. Magn. Reson. 248 (2014) 81–95, https://doi.org/10.1016/j.jmr.2014.09.014.
[20] T. Gopinath, G. Veglia, 3D DUMAS: Simultaneous acquisition of three-dimensional magic angle spinning solid-state NMR experiments of proteins, J. Magn. Reson. 220 (2012) 79–84, https://doi.org/10.1016/j.jmr.2012.04.006.
[21] K. Sharma, P.K. Madhu, K.R. Mote, A suite of pulse sequences based on multiple sequential acquisitions at one and two radiofrequency channels for solid-state magic-angle spinning NMR studies of proteins, J. Biomol. NMR. 65 (3-4) (2016) 127–141, https://doi.org/10.1007/s10858-016-0043-z.
[22] T. Gopinath, G. Veglia, Orphan spin operators enable the acquisition of multiple 2D and 3D magic angle spinning solid-state NMR spectra, J. Chem. Phys. 138 (18) (2013) 184201, https://doi.org/10.1063/1.4803126.
[23] A. Gallo, W.T. Franks, J.R. Lewandowski, A suite of solid-state NMR experiments to utilize orphaned magnetization for assignment of proteins using parallel high and low gamma detection, J. Magn. Reson. 305 (2019) 219–231, https://doi.org/10.1016/j.jmr.2019.07.006.
[24] J.R. Lewandowski, H.J. Sass, S. Grzesiek, M. Blackledge, L. Emsley, Site-specific measurement of slow motions in proteins, J. Am. Chem. Soc. 133 (42) (2011) 16762–16765, https://doi.org/10.1021/ja206815h.
[25] A.G. Palmer, F. Massi, Characterization of the dynamics of biomacromolecules using rotating-frame spin relaxation NMR spectroscopy, Chem. Rev. 106 (5) (2006) 1700–1719, https://doi.org/10.1021/cr0404287.
[26] N. Giraud, M. Blackledge, M. Goldman, A. Böckmann, A. Lesage, F. Penin, L. Emsley, Quantitative analysis of backbone dynamics in a crystalline protein from nitrogen-15 spin-lattice relaxation, J. Am. Chem. Soc. 127 (51) (2005) 18190–18201, https://doi.org/10.1021/ja055182h10.1021/ja055182h.s001.
[27] J.R. Lewandowski, J. Sein, H.J. Sass, S. Grzesiek, M. Blackledge, L. Emsley, Measurement of site-specific 13C spin-lattice relaxation in a crystalline protein, J. Am. Chem. Soc. 132 (24) (2010) 8252–8254, https://doi.org/10.1021/ja102744b.
[28] W.T. Franks, D.H. Zhou, B.J. Wylie, B.G. Money, D.T. Graesser, H.L. Frericks, G. Sahota, C.M. Rienstra, Magic-angle spinning solid-state NMR spectroscopy of the β1 immunoglobulin binding domain of protein G (GB1): ^{15}N and ^{13}C chemical shift assignments and conformational analysis, J. Am. Chem. Soc. 127 (2005) 12291–12305, https://doi.org/10.1021/ja044497e.
[29] R. Stevens, The Development of Solid-state NMR Methodology to Study the Dynamics of Proteins and Ice, University of Warwick, 2018.
[30] Y.T. van den Hoogen, S.J. Treurniet, H.C.P.F. Roelen, E. de Vroom, G.A. van der Marel, J.H. van Boom, C. Altona, Conformational analysis of the

tetranucleotides m_2^6A–m_2^6A-U-m_2^6A (m_2^6A =N^6-dimethyladenosine) and U-m_2^6A-U-m_2^6A and of the hybrid dA-r(U-A): A one- and two-dimensional NMR study, Eur. J. Biochem. 171 (1-2) (1988) 155–162, https://doi.org/10.1111/ejb.1988.171.issue-1-210.1111/j.1432-1033.1988.tb13771.x.

[31] D.S. Wishart, C.G. Bigam, J. Yao, F. Abildgaard, H.J. Dyson, E. Oldfield, J.L. Markley, B.D. Sykes, ^{1}H, ^{13}C and ^{15}N chemical shift referencing in biomolecular NMR, J. Biomol. NMR. 6 (2) (1995) 135–140.

[32] D. Marion, M. Ikura, R. Tschudin, A.d. Bax, Rapid recording of 2D NMR spectra without phase cycling. Application to the study of hydrogen exchange in proteins, J. Magn. Reson. 85 (2) (1989) 393–399, https://doi.org/10.1016/0022-2364(89)90152-2.

[33] Z. Zhou, R. Kümmerle, X. Qiu, D. Redwine, R. Cong, A. Taha, D. Baugh, B. Winniford, A new decoupling method for accurate quantification of polyethylene copolymer composition and triad sequence distribution with ^{13}C NMR, J. Magn. Reson. 187 (2) (2007) 225–233, https://doi.org/10.1016/j.jmr.2007.05.005.

[34] D.H. Zhou, C.M. Rienstra, High-performance solvent suppression for proton detected solid-state NMR, J. Magn. Reson. 192 (1) (2008) 167–172, https://doi.org/10.1016/j.jmr.2008.01.012.

[35] T. Gopinath, G. Veglia, Dual acquisition magic-angle spinning solid-State NMR-spectroscopy: Simultaneous acquisition of multidimensional spectra of biomacromolecules, Angew. Chemie - Int. Ed. 51 (11) (2012) 2731–2735, https://doi.org/10.1002/anie.201108132.

[36] R. Kurbanov, T. Zinkevich, A. Krushelnitsky, The nuclear magnetic resonance relaxation data analysis in solids: General $R_1/R_{1\rho}$ equations and the model-free approach, J. Chem. Phys. 135 (2011), https://doi.org/10.1063/1.3658383.

[37] A. Grommek, B.H. Meier, M. Ernst, Distance information from proton-driven spin diffusion under MAS, Chem. Phys. Lett. 427 (4-6) (2006) 404–409, https://doi.org/10.1016/j.cplett.2006.07.005.

[38] N. Giraud, M. Blackledge, A. Böckmann, L. Emsley, The influence of nitrogen-15 proton-driven spin diffusion on the measurement of nitrogen-15 longitudinal relaxation times, J. Magn. Reson. 184 (1) (2007) 51–61, https://doi.org/10.1016/j.jmr.2006.09.015.

[39] S. Asami, J.R. Porter, O.F. Lange, B. Reif, Access to Cα backbone dynamics of biological solids by^{13}C T_1 Relaxation and molecular dynamics simulation, J. Am. Chem. Soc. 137 (3) (2015) 1094–1100, https://doi.org/10.1021/ja509367q.

[40] A. Krushelnitsky, T. Bräuniger, D. Reichert, ^{15}N spin diffusion rate in solid-state NMR of totally enriched proteins: The magic angle spinning frequency effect, J. Magn. Reson. 182 (2) (2006) 339–342, https://doi.org/10.1016/j.jmr.2006.06.028.

[41] M.D. Sørensen, A. Meissner, O.W. Sørensen, Spin-state-selective coherence transfer via intermediate states of two-spin coherence in IS spin systems: Application to E.COSY-type measurement of J coupling constants, J. Biomol. NMR. 10 (1997) 181–186, https://doi.org/10.1023/A:1018323913680.

[42] A. Vallet, A. Favier, B. Brutscher, P. Schanda, ssNMRlib: a comprehensive library and tool box for acquisition of solid-state nuclear magnetic resonance experiments on Bruker spectrometers, Magn. Reson. 1 (2) (2020) 331–345, https://doi.org/10.5194/mr-1-331-202010.5194/mr-1-331-2020-supplement.

[43] J. Sein, N. Giraud, M. Blackledge, L. Emsley, The role of ^{15}N CSA and CSA/dipole cross-correlation in (15)N relaxation in solid proteins, J. Magn. Reson. 186 (1) (2007) 26–33, https://doi.org/10.1016/j.jmr.2007.01.010.

[44] V. Chevelkov, A.V. Zhuravleva, Y.i. Xue, B. Reif, N.R. Skrynnikov, Combined analysis of ^{15}N relaxation data from solid- and solution-state NMR spectroscopy, J. Am. Chem. Soc. 129 (42) (2007) 12594–12595, https://doi.org/10.1021/ja073234s10.1021/ja073234s.s001.

[45] L.E. Kay, T.E. Bull, L.K. Nicholson, C. Griesinger, H. Schwalbe, A. Bax, D.A. Torchia, The measurement of heteronuclear transverse relaxation times in ax3 spin systems via polarization-transfer techniques, J. Magn. Reson. 100 (3) (1992) 538–558, https://doi.org/10.1016/0022-2364(92)90058-F.

[46] U. Sternberg, R. Witter, I. Kuprov, J.M. Lamley, A. Oss, J.R. Lewandowski, A. Samoson, ^{1}H line width dependence on MAS speed in solid state NMR – Comparison of experiment and simulation, J. Magn. Reson. 291 (2018) 32–39, https://doi.org/10.1016/j.jmr.2018.04.003.

[47] J.M. Lamley, D. Iuga, C. Öster, H.-J. Sass, M. Rogowski, A. Oss, J. Past, A. Reinhold, S. Grzesiek, A. Samoson, J.R. Lewandowski, Solid-State NMR of a Protein in a Precipitated Complex with a Full-Length Antibody, J. Am. Chem. Soc. 136 (48) (2014) 16800–16806, https://doi.org/10.1021/ja5069992.

[48] S.J. Page, A. Gallo, S.P. Brown, J.R. Lewandowski, J.V. Hanna, W.T. Franks, Simultaneous MQMAS NMR Experiments for Two Half-Integer Quadrupolar Nuclei, J. Magn. Reson. 320 (2020) 106831, https://doi.org/10.1016/j.jmr.2020.106831.